Al-Furat Journal of Innovations in Mechanical and Sustainable Energy Engineering (FJIMSE)

Combined Experimental and Numerical Investigation of Geometric Parameters on the Performance of Savonius Vertical Axis Wind Turbine

Qusay Mohammed Jabbar Al-Atwani
Master's student at the College of Engineering Technology / Najaf/ Al-Furat Al-Awsat University
zechariahqusay@gmail.com

ABSTRACT. *Wind energy has become one of the most widely deployed renewable sources because it is scalable, mature, and suitable for both utility-scale and distributed generation applications. This work investigates the aerodynamic development and experimental validation of a Savonius vertical-axis wind turbine (VAWT) intended for low to medium wind-speed applications. A complete workflow was adopted starting from a validated CFD model, followed by systematic geometric development, optimal design selection, additive manufacturing, and wind-tunnel-style testing, then concluding with a direct comparison between numerical and experimental results. The CFD simulations were conducted in ANSYS-CFX using air at* $25°C$ *and 1 atm, and the turbulence model* $k-\omega$ *SST. Model validation was first performed at an inlet wind speed of* $9\,m/s$ *using the optimal reference configuration reported in the literature (OR0.109BS2BN2). After validation, the baseline turbine was analyzed at* $5\,m/s$ *and used as the starting point for parametric development. Three geometric variables were introduced and varied in a controlled one-factor-at-a-time strategy: the upper tilt angle* $\beta(0°-12°, 1°$ *step), the blade orientation angle*$\gamma(0°-120°)$*, and an arc-edge parameter* r_v *(100-500 with stepwise 100 increments). The results showed that* β *reduced performance across the tested range; therefore,* $\beta = 0°$ *was retained. In contrast,* γ *had the strongest influence and increased reaching*$C_P \approx 0.2716$*. The effect of* r_v *was comparatively weak, producing only minor changes once* γ *was optimized. The optimum turbine was fabricated using 3D printer with Hyper PLA material. A low-medium wind-speed blower test rig was designed and built to generate uniform flow in the range of* $5-9\,m/s$*. Experimental performance curves were produced at* $5\,m/s$*, and the trends matched the CFD predictions: the power coefficient increased with TSR up to an optimum region around* $\lambda \approx 1.0$*, then decreased at higher TSR. The peak experimental value was approximately* $C_P \approx 0.259$ *near* $\lambda \approx 1.0$*, compared with a corresponding CFD peak near* $C_P \approx 0.272$*. The remaining differences are attributed to practical effects not fully represented in the numerical model, including mechanical losses, manufacturing tolerances, surface roughness, and measurement uncertainty. The combined CFD-experimental methodology successfully identified an improved Savonius rotor configuration and demonstrated a consistent validation-to-optimization workflow suitable for small-scale wind energy harvesting.*

Keywords: Vertical axis wind turbine, Savonius, performance, wind tunnel.

1. Introduction

The global energy sector is undergoing a significant transition toward sustainable and low-carbon energy systems due to increasing environmental concerns, climate change policies, and the depletion of conventional fossil fuel resources [1,2]. Among the available renewable energy technologies, wind energy has become one of the most widely utilized sources because of its scalability, technological maturity, and suitability for both large-scale and distributed generation systems [1,2]. In recent years, particular

attention has been given to small-scale wind energy applications in urban environments, remote regions, and hybrid microgrid systems, where localized generation improves system reliability and reduces dependence on centralized power infrastructure [3]. Wind turbines are generally classified into two main categories: Horizontal Axis Wind Turbines (HAWTs) and Vertical Axis Wind Turbines (VAWTs), based on their axis of rotation and aerodynamic operating principles [4]. HAWTs dominate global wind energy production due to their relatively high aerodynamic efficiency, with practical power coefficient values reaching approximately 0.48 [**5**]. However, their operation requires continuous alignment with wind direction through yaw mechanisms, in addition to tall tower installations, which increase structural complexity, maintenance requirements, and cost [4,5]. Moreover, HAWTs are less effective in highly turbulent or multidirectional wind conditions, such as those encountered in urban environments. In contrast, VAWTs offer several advantages, including omnidirectional wind acceptance, simpler mechanical design, and the ability to locate heavy components near ground level, which reduces structural loads and facilitates maintenance [5,6]. Among VAWTs, the Savonius turbine is one of the most widely studied configurations due to its simple construction, robustness, low cost, and excellent self-starting capability under low wind speed conditions [6,7,8]. The Savonius rotor operates based on drag forces generated by the pressure difference between the concave advancing blade and the convex returning blade. This mechanism enables stable operation even under fluctuating wind directions. Despite these advantages, the aerodynamic efficiency of Savonius turbines is relatively low compared with lift-based turbines. Typical power coefficient values range between 0.1 and 0.15, which is significantly lower than the theoretical Betz limit of 59.3% for wind energy extraction [9,10]. This limitation is primarily attributed to several complex aerodynamic phenomena, including flow separation, vortex shedding, wake interaction, and the generation of negative torque on the returning blade [8,11]. These effects are more pronounced at low to moderate Reynolds numbers and specific tip speed ratio (TSR) ranges, which are characteristic of small-scale Savonius turbine applications [12].To address these limitations, numerous studies have investigated performance enhancement techniques through geometric modifications and flow control strategies. These include variations in blade number [13,14], overlap ratio and blade interference [15,16], blade profile modifications such as helical, elliptical, and twisted designs [17–18], multistage configurations [17,19], and the use of augmentation devices such as deflectors and flow-guiding systems [20,21,22]. These approaches aim to improve torque generation, enhance pressure distribution, and reduce negative aerodynamic effects on the returning blade. However, despite the extensive body of research, the reported results remain inconsistent and sometimes contradictory due to differences in experimental conditions, numerical modeling approaches, and turbine configurations [23,24]. Many studies focus on single-parameter optimization, neglecting the coupled and nonlinear interactions between multiple geometric variables. Furthermore, the accuracy of computational fluid dynamics (CFD) predictions is not always validated through comprehensive experimental comparisons under consistent operating conditions, particularly for three-dimensional unsteady simulations [7,25]. Therefore, there is a clear need for an integrated research framework that combines validated numerical modeling with systematic geometric optimization and experimental verification. Such an approach is essential for identifying reliable and practically applicable design improvements. Accordingly, the present study aims to investigate the combined influence of key geometric parameters on the performance of a Savonius-type vertical axis wind turbine

ATU- FJIMSE, Vol. 4 No. 1 (2026): volume 4,Issu 1,May 2026 , All Rights Reserved

using both CFD simulations and experimental testing. The study establishes a comprehensive workflow that includes model validation, parametric development, prototype fabrication, and experimental evaluation, thereby addressing the key research gaps identified in the literature and contributing to the advancement of small-scale wind energy systems

2. Methodology

2.1 Validation of model (base design model)

In order to ensure the reliability and accuracy of the numerical methodology adopted in this study, a validation process was first carried out using a well-documented Savonius turbine configuration reported in the literature [25] . The selected reference model corresponds to the configuration denoted as (OR0.109BS2BN2), which represents the optimal design in the cited study in terms of power coefficient performance. This configuration is characterized by an overlap ratio of 0.109, a two-bladed rotor, and the blade shape labeled as BS2 in the reference work.

The base design model was reconstructed in full three-dimensional form using SolidWorks 2025 extracted from the reference study, as shown in Figure 3.2. This figure illustrates the reconstructed Savonius rotor used for the validation process and serves as the baseline configuration for all new subsequent numerical developments in this research.

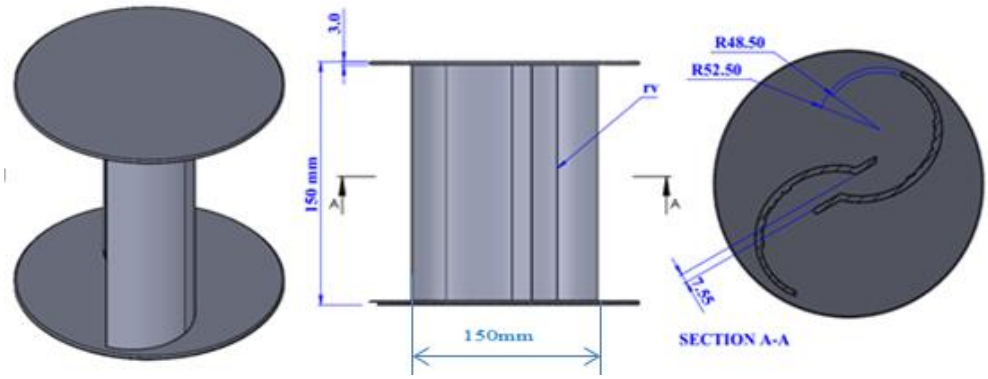

Figure 2-1: Three-dimensional geometry of the base Savonius turbine model used for CFD validation.

The numerical simulation of the base model was performed using ANSYS CFX under operating conditions to those reported in the reference study [25]. The maximum power coefficient obtained from the present CFD simulation was found to be (CP = 0.268). This value shows good agreement with the reference value of (CP = 0.27001) reported for the same configuration, resulting in deviation of approximately 0.37%. This small variance can be attributed to differences in grid resolution, numerical schemes, and turbulence modeling assumptions, which are commonly observed in computational fluid dynamics-based wind turbine analyses.

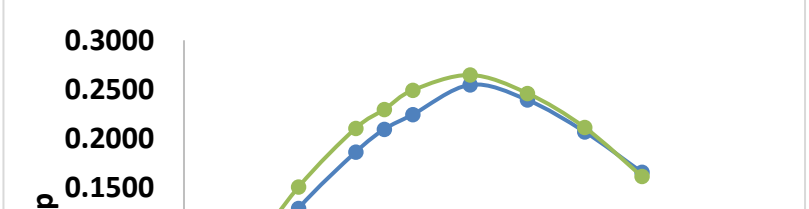

Figure2-2: Result of Validation model at v= 9 m/s

After completing the validation at $= 9\ m/s$, the same numerical setup was applied at a lower inlet speed of $V = 5\ m/s$ to generate a consistent baseline curve for the remainder of the thesis development work. The resulting performance curve is presented in Figure 4.2, which reports the same trend observed at $9\ m/s$: C_P increases with λ up to an optimum and then decreases as λ becomes larger. Figure 4.2: Result of Simulation model at $= 5\ m/s$. At $= 5\ m/s$, the simulated power coefficient increases from 0.0537 at $\lambda = 0.2$ to a peak value of 0.2503 at $\lambda = 1.0$ (baseline case), followed by a progressive reduction to 0.2351,0.2032, and 0.1625 at $\lambda = 1.2$,1.4, and 1.6 , respectively. The torque and power values scale down as expected due to the lower wind kinetic power available, but the nondimensional indicators (especially C_P and C_Q) remain within the same practical range, indicating that the rotor aerodynamic behavior is preserved under the lower-speed operating condition. Importantly, this $5\ m/s$ curve was used as the working operating condition for the design-development stage and for ensuring consistency with the experimental testing speed adopted later in the study.

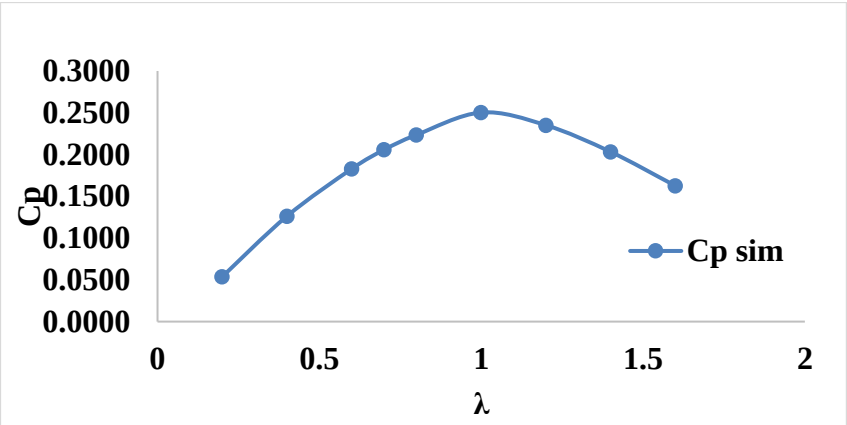

Figure 2-3: Result of Simulation model at v=5 m/s

2.2 Simulation work

The numerical investigation in this chapter was performed using three-dimensional unsteady Computational Fluid Dynamics (CFD) in ANSYS CFX (R2) to predict the aerodynamic torque and the corresponding power coefficient of the Savonius rotor. The simulations were executed on a workstation equipped with an AMD Ryzen™ 9 7950X (16-core, up to 5.7 GHz) processor, 64 GB RAM, NVIDIA RTX 3090 GPU, and Windows 10 (64-bit). The overall CFD workflow followed the standard sequence of pre-processing, solving, and post-processing. In the pre-processing stage, the turbine geometry and computational domains were prepared, and the fluid region was divided into two sub-domains to represent rotor motion: a stationary (fixed) outer air domain and an inner rotating rotor air domain, as shown in Figure 2.4. This allows the rotor to rotate relative to the surrounding flow while keeping the far-field boundaries stationary, and it enables robust transient simulations through an appropriate rotor–stator interface treatment between the two domains. In the solver stage, the governing conservation equations of mass and momentum were solved in a transient manner until periodic rotor behavior was obtained, while ensuring adequate convergence at each time step. At last, in the post-processing stage, the instantaneous and cycle-averaged torque were extracted to compute turbine performance indicators, including the power coefficient, and to support the validation and subsequent parametric investigations presented in the following sections.

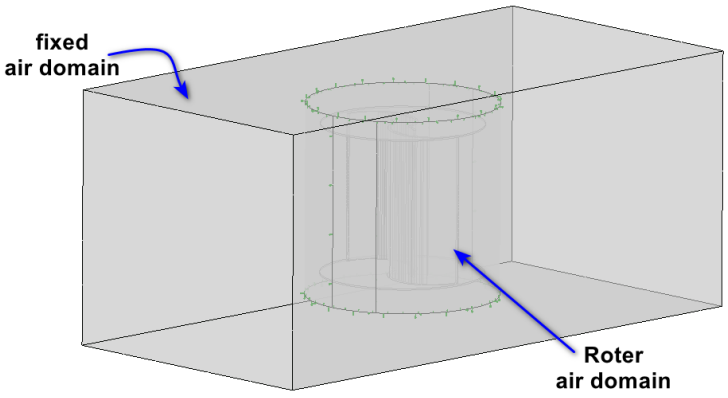

Figure 2-4: Computational domain arrangement used for the CFD simulations, consisting of a stationary outer air domain and an inner rotating rotor air domain.

2.3 Mesh independence for domain

Mesh independence was carried out to ensure that the predicted aerodynamic performance is not affected by the spatial discretization and that the computed power coefficient remains stable with further grid refinement. A series of structured refinement trials were performed for the full 3D computational domain in ANSYS CFX, where the mesh density was gradually increased while keeping the boundary conditions and solver settings unchanged. The objective was to identify a mesh that provides an accurate solution at a reasonable computational cost, without unnecessary refinement. Table 2.1 summarizes the mesh statistics for the five tested grids, including the total number of elements and nodes, as well as mesh quality indicators (skewness and orthogonal quality). The generated meshes maintained a consistently high orthogonal quality (~0.99) across all trials, indicating good alignment of elements with the local geometry and limited numerical diffusion. Although skewness increased slightly with refinement, the values remained within an acceptable range for reliable CFD simulations, confirming that element distortion was not severe enough to compromise solution accuracy.

Table 2-1: Statistical grid-independence assessment for the 3D computational domain.

Trial	No. of elements	No. of nodes	Skewness	Orthogonal quality
1	92388	135418	0.67144	0.99
2	119199	368702	0.71017	0.99
3	264813	629158	0.74258	0.99
4	587874	917752	0.74301	0.99
5	974385	1606066	0.75017	0.99

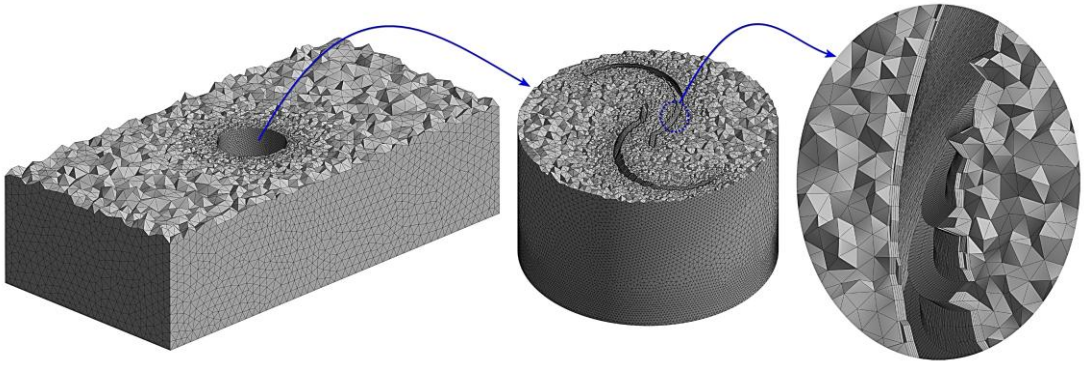

Figure 2-5 Mesh of optimum design Error! No text of specified style in document.

2.4 Boundary conditions of turbine domain

The boundary conditions for the turbine CFD domain were implemented in accordance with the validated wind-tunnel-based setup reported in the reference for the optimal OR0.109BS2BN2 [61]. As shown in Figure 2.6, the computational region was divided into two sub-domains: (i) a fixed (stationary) outer air domain representing the wind-tunnel test section, and (ii) a rotating cylindrical rotor air domain enclosing the turbine. A uniform inlet velocity of $9\,m/s$ was prescribed at the upstream boundary, while an outlet pressure boundary (static-pressure outlet) was imposed downstream; the tunnel boundaries and all turbine solid surfaces were treated as no-slip walls. The rotating sub-domain diameter was selected as 1.1D (150 mm) to properly encompass the rotor while maintaining stable rotor-stator coupling. Rotor motion was imposed through an angular velocity consistent with the tip-speed ratio definition $\mathrm{TSR} = \omega R/V_\infty$, and the performance comparison/optimization cases were evaluated at $\mathrm{TSR} = 1$ (i.e., $\omega = V_\infty/R$) to standardize assessment across designs. The interface between stationary and rotating domains followed a rotor-stator strategy (initialized using a frozen-rotor solution and then advanced using a transient rotor-stator (TRS 360) formulation) to capture the unsteady interaction between the two domains. Finally, the unsteady RANS solution (SST $k-\omega$) was advanced with a residual target of 10^{-4}, using 40 time-steps per revolution with 1-3 inner iterations per time-step, and solution statistics were taken after reaching a periodic regime (≈ four revolutions)

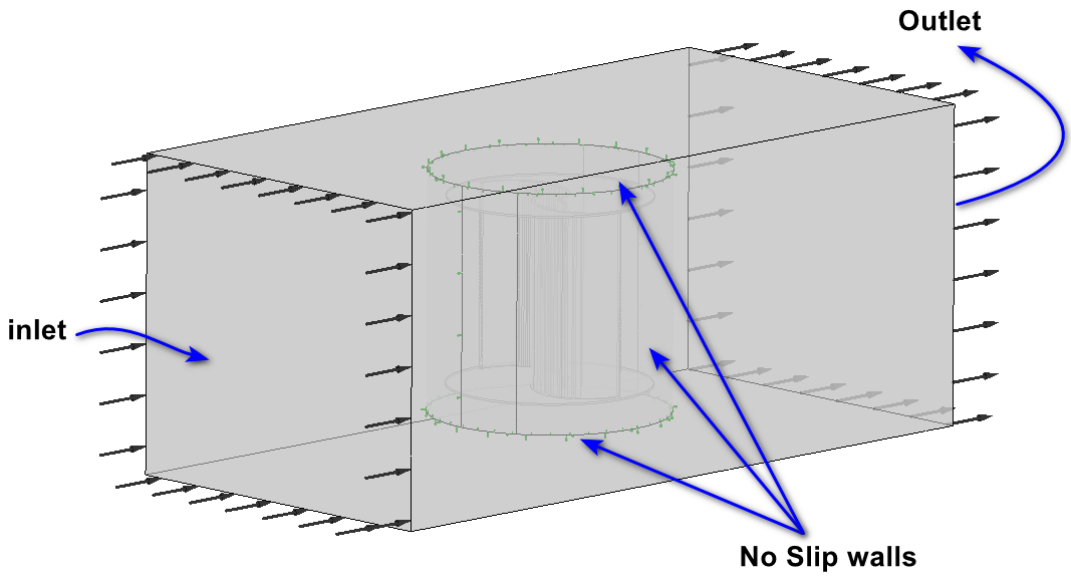

Figure2-6: Boundary conditions of domain

ATU- FJIMSE, Vol. 4 No. 1 (2026): volume 4,Issu 1,May 2026 , All Rights Reserved

2.5 Develop the Turbine Geometrical Specifications

The Savonius rotor was first built as a 3D CAD model. The main dimensions and the general shape of the rotor (including the end plates and blade profile details) are shown in Figure 3.7. After that, the model was prepared as a parametric design so that the geometry could be changed and tested in a clear and organized way during the CFD work.

Three geometric parameters were selected for development:

- **β (beta): the upper inclination angle applied from the top side of the rotor**
- **γ (gamma): the blade orientation (rotation) angle**
- **r_v : an arc parameter used to control the blade curvature shape**

The selected ranges were chosen to be realistic for manufacturing and also consistent with the CFD validation setup. The parameters were tested as follows: β was changed from $0°$ to $12°$ with a step of $1°$, γ was changed from $0°$ to $120°$ with a step of $10°$ (and extra tests near the best values), and r_v was changed from $100°$ to $500°$ with a step of $100°$. A step-by-step strategy was used to clearly see the effect of each parameter. First, β was tested while keeping $\gamma = 0°$ and $r_v = 0°$. The results (models M1-M13 in Table 3.2) showed that all nonzero β values gave a lower C_P than the baseline model. For this reason, β was fixed at $0°$, and the baseline model M 1 was kept as the reference case with $C_P = 0.2503$. Next, with $\beta = 0°$ and $r_v = 0°$, the angle γ was tested from $0°$ to $120°$ (models M14-M25). In this stage, C_P increased clearly as γ increased, especially after $90°$. For example, C_P reached 0.2697 at $\gamma = 100°$ (M23) and 0.2708 at $\gamma = 110°$ (M24). Since the values between $110°$ and $120°$ showed a rise and then a small drop, additional tests were done in this region, and the best value was found at $\gamma = 118°$, where $C_P = 0.2715$ (model M25). Finally, after fixing the angles at the upper range, the arc parameter r_v was investigated (models M26-M37). When $\beta = 0°$ and $\gamma = 120°$, changing r_v from $10°$ to $120°$ caused only small changes in C_P. The results stayed almost constant between 0.270 and 0.2712, which shows that r_v has a smaller effect compared to γ for this rotor design. Based on these results, the best model in this development stage was $M25(\beta = 0°, \gamma = 118°, r_v = 0°)$, and it was selected as the final design to continue with the next steps of the thesis (manufacturing and experimental testing). The full list of models and results is given in Table 2.2, and the rotor geometry is shown in Figure 2.7.

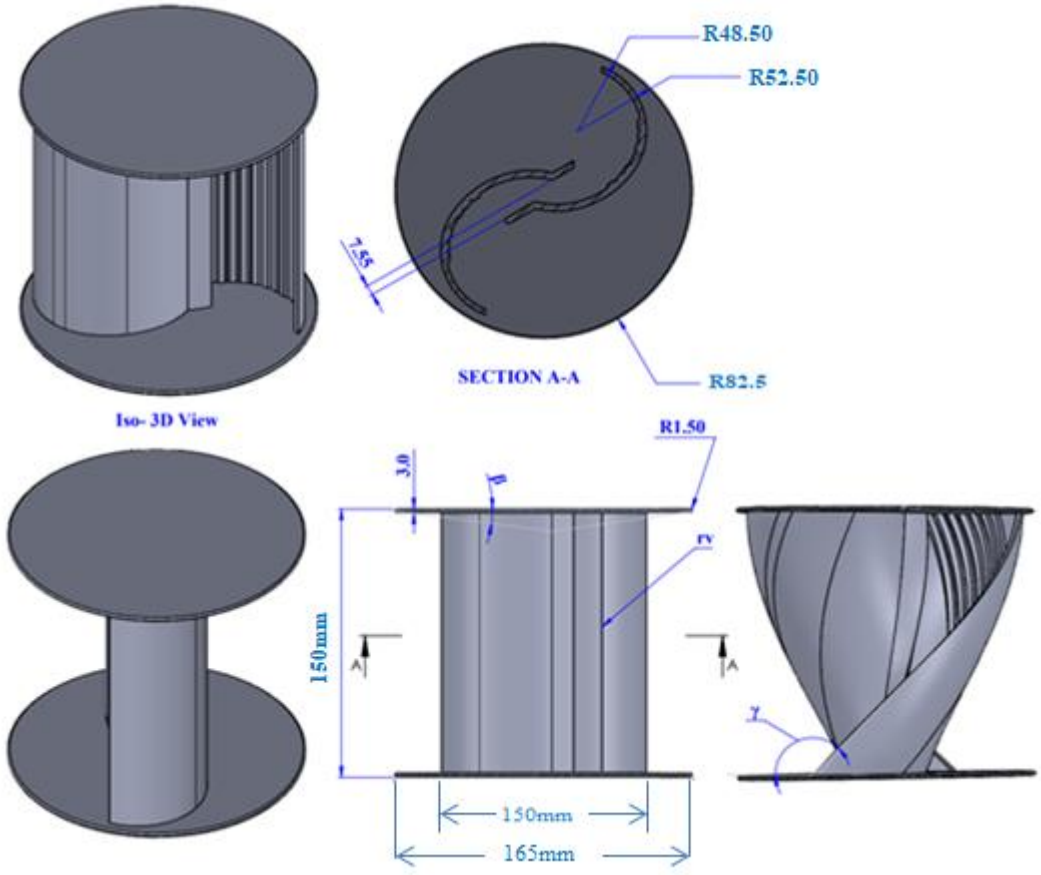

Figure2-7:Geometry and parameter design

Table2-2: Basic parameters adopted

Parameter	Meaning	Range	Step
β	Top angle	0° → 12°	1°
γ	Blade rotation angle	10° → 120°	10° (then refined)
(rv)	Arc parameter	100 → 500 mm	100 mm

Table 2-2: Parametric development matrix and resulting power coefficient C_P for variations of β, γ, and r_v.

B: St

0° **12°**

γ: Step=1(

10° **120°**

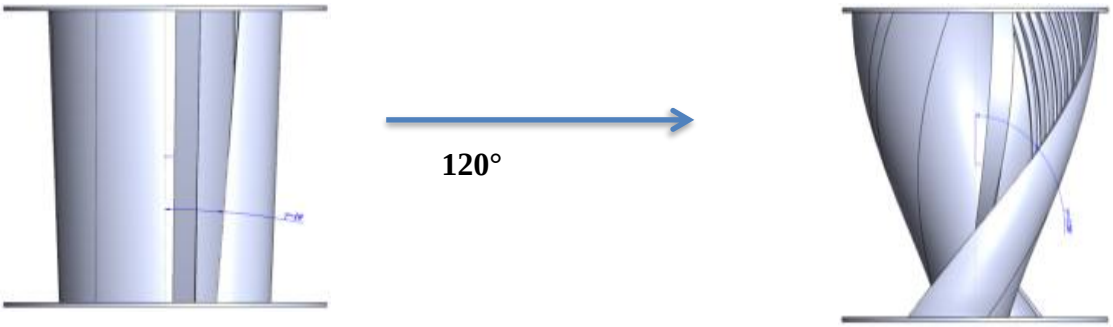

rv: Step=

100 **500 mm**

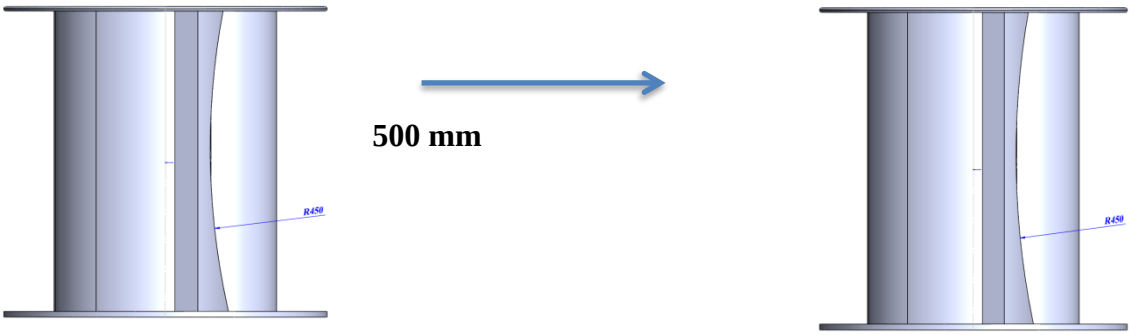

Test	β	γ	rv	cp
M0	0	0	0	0.2503
M1	1	0	0	0.243
M2	2	0	0	0.2425
M3	3	0	0	0.2418
M4	4	0	0	0.2464
M5	5	0	0	0.2347
M6	6	0	0	0.2417
M7	7	0	0	0.2397
M8	8	0	0	0.2447
M9	9	0	0	0.2418
M110	10	0	0	0.2477
M11	11	0	0	0.2374
M12	12	0	0	0.2317

Test	β	γ	rv	cp
M13	0	10	0	0.2508
M14	0	20	0	0.2511
M15	0	30	0	0.2513
M16	0	40	0	0.2572
M17	0	50	0	0.2591
M18	0	60	0	0.2595
M19	0	70	0	0.2601
M20	0	80	0	0.2604
M21	0	90	0	0.2617
M22	0	100	0	0.2697
M23	0	110	0	0.2708
M24	0	118	0	0.2716
M25	0	120	0	0.2701

Test	β	γ	rv	cp
M26	0	118	100	0.2707
M27	0	118	200	0.2709
M28	0	118	300	0.2708
M29	0	118	400	0.2709
M30	0	118	450	0.2710
M31	0	118	500	0.2710

The change in the arc (rv) occurred after changing the angle of the edge and obtaining the best result of cp, which was 0.716. This means that the edge angle (γ) remained constant at 118 degrees and the arc began to change to obtain the best desired result. Figures 3.9 shows the optimal edge angle.

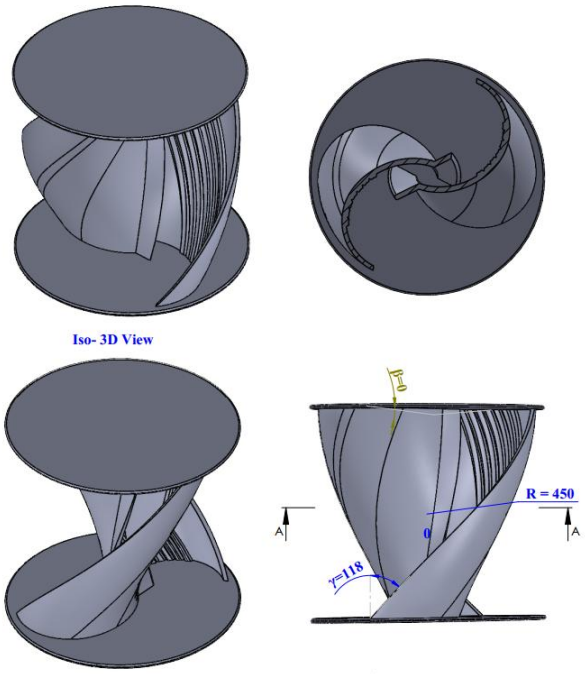

Figure 2-8: Optimum design of savonius turbine after twist

2.6 Experimental work

2.6.1 Fabrication of the Low- medium wind Speed Blower

The low-to-medium wind speed blower (wind tunnel) was designed and fabricated as a laboratory system to provide controlled airflow conditions suitable for testing the Savonius wind turbine. It was constructed in two separable sections for ease of assembly, maintenance, and turbine installation. The blower section included a centrifugal fan rated at 3 hp to generate airflow, an air filter tube network acting as a flow straightener to improve flow uniformity, and a wind-speed control gate to regulate velocity. The control gate featured movable vanes connected to a lever, allowing precise adjustment of the airflow passage area, which in turn controlled the wind speed directed toward the turbine. The gate was mounted on a graduated linear scale (0 to 12 cm), enabling repeatable settings corresponding to specific calibrated wind speeds. To enhance the quality and uniformity of the incoming flow, a honeycomb-like flow straightener composed of multiple short tubes was installed upstream of the test section. Overall, this controlled blower setup produced consistent and uniform flow conditions in the range of approximately 4 to 7 m/s for reliable experimental performance testing of the Savonius turbine shown in Figure (3.11).

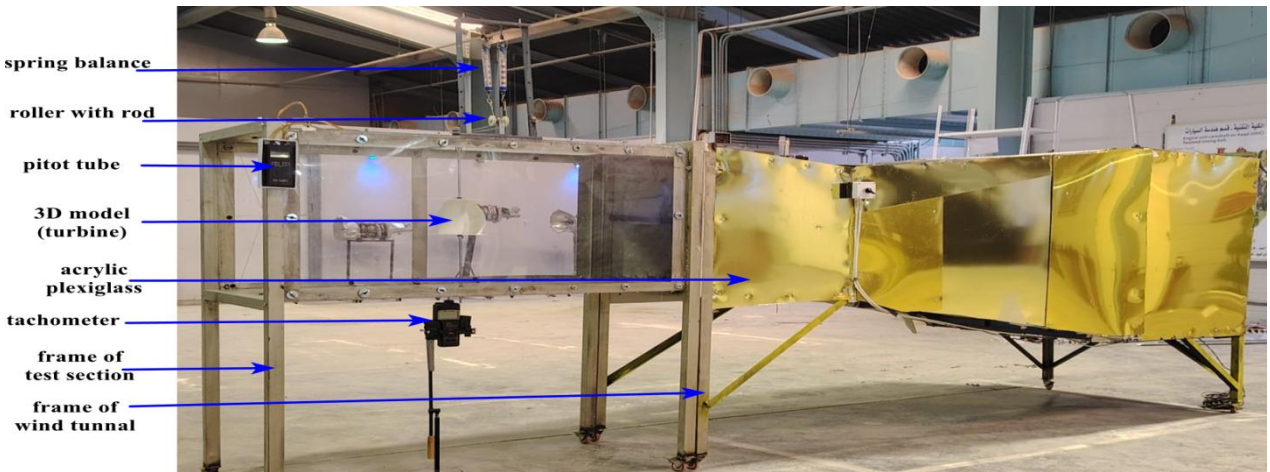

Figure 2-9: Experimental Setup in Open-Type Wind

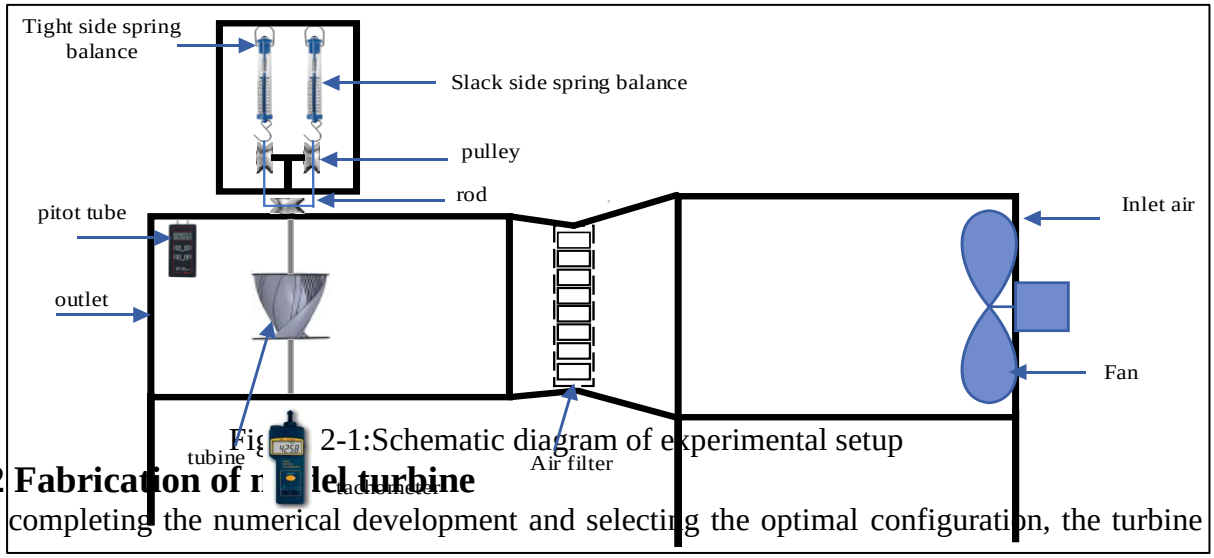

Fig 2-1:Schematic diagram of experimental setup

2.6.2 Fabrication of r lel turbine

After completing the numerical development and selecting the optimal configuration, the turbine geometry was prepared for manufacturing using SolidWorks 2025. The final CAD model was exported for additive manufacturing, and the optimal turbine was fabricated using a 3D printer to ensure accurate reproduction of the designed blade profile and rotor details. The turbine model was printed using Hyper PLA (Hyper-PLA) filament. Printing was performed on a Creality Ender-3 V3 3D printer, and the total printing time was approximately 13 hours. After printing, the model was checked visually and dimensionally (as possible) to ensure the rotor blades, end plates, and overall shape matched the design intent. Any minor post-processing (e.g., removing supports and cleaning edges) was performed to ensure smooth assembly and safe testing. The manufactured turbine geometry are illustrated in the turbine drawing provided in Figure 3.21

Figure2-2:Manufactured turbine model geometry in 3D printer.

2.7 Experimental setup

The experimental setup consisted of the blower test section, the mounted turbine model, and a set of measuring instruments for wind speed, rotational speed, and torque. During testing, the wind speed was controlled using the blower control unit and verified using two methods:

- Digital anemometer for direct speed measurement, and
- Pitot tube for calibration and validation of the measured velocity, as shown in Figure 2.12

To confirm that the outlet flow was uniform and the measurements were reliable, the exit cross-section was divided into multiple regions using a string grid, and the wind speed was measured at several points across the section. This method ensured that the reported wind speed represented the real flow entering the turbine and helped verify the high uniformity level achieved by the flow straightener. For each test condition, the wind speed was set to approximately 5, 6, 7, and 9 m/s. At each speed, the turbine rotational speed was recorded simultaneously. Rotor speed was measured using a digital tachometer and an RPM sensor, and both instruments were used to increase measurement confidence through cross-checking and calibration. The RPM measurement approach. Mechanical torque was determined using the rope-and-pulley (brake) method. A pulley was attached to the main shaft, and a rope was wrapped around it. During the experiment, a controlled load was applied by tightening one side of the rope and maintaining the other side as the slack side. The torque was calculated from the load difference and the effective pulley radius (as described in the theoretical Section 3.6). Each experiment was repeated multiple times under the same conditions, and consistent readings were used to reduce random error and improve repeatability.

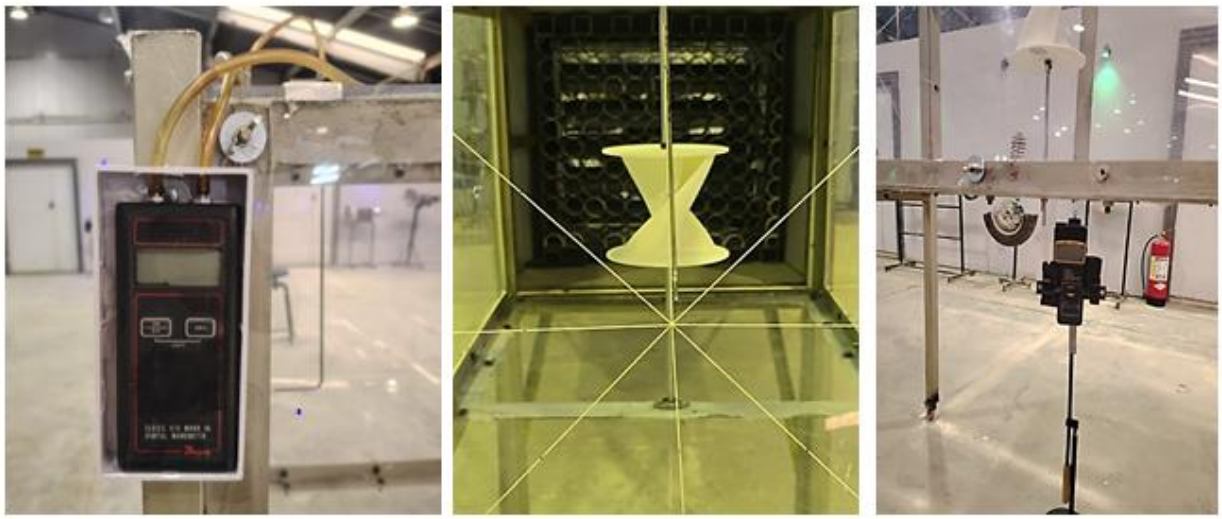

(a) (b) (c)

Figure2.12:(a): Pitot tube for calibration (b):multiple regions using a string grid(c):Measurement of turbine rotational speed using a tachometer / RPM sensor (calibrated).

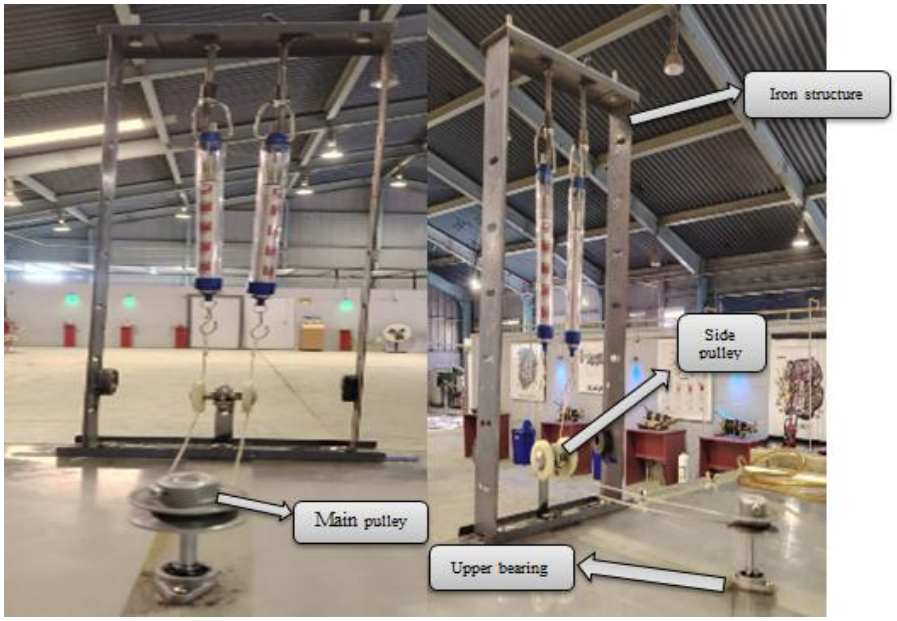

Figure 2-12:Measurement of turbine rotational speed using a tachometer / RPM sensor (calibrated).

2.8 Wind turbine performance and power calculations

Wind turbine performance is commonly evaluated by comparing the useful mechanical power produced by the rotor to the available kinetic power in the incoming wind. In this study, rotor power was determined from the measured torque and the rotor angular velocity, while the non-dimensional performance indicators (such as C_P and C_T) were calculated using standard wind-energy relations

Available Wind Power

The kinetic power available in the wind that crosses the turbine swept area is given by:

$$P_{\text{wind}} = \frac{1}{2}\rho A V_\infty^3 \qquad (3.1)$$

where ρ is air density (kg/m^3), A is the swept area (m^2), and V_∞ is the free-stream wind speed (m/s).

For a vertical-axis wind turbine (VAWT) such as a Savonius rotor, the swept area is:

$$A = DH$$

where D is rotor diameter (m) and H is rotor height (m).

Rotor Angular Velocity and Tip Speed Ratio

The rotor angular velocity ω can be obtained from the rotational speed (rpm) :

$$\omega = \frac{2\pi N}{60} \qquad (3.3)$$

The tip speed ratio (TSR) is a key non-dimensional parameter in wind turbine analysis and is defined as:

$$\lambda = \frac{\omega R}{V_\infty} \qquad (3.4)$$

where $R = D/2$ is rotor radius (m).

Mechanical Power Output

The mechanical power extracted by the turbine shaft is computed from the torque T and angular velocity :

$$P_{out} = T\omega \qquad (3.5)$$

ATU- FJIMSE, Vol. 4 No. 1 (2026): volume 4,Issu 1,May 2026 , All Rights Reserved

where T is the measured turbine torque (N).

Power Coefficient

Because not all wind power can be extracted by the rotor (due to wake losses, flow separation, and aerodynamic drag effects), turbine performance is usually expressed using the power coefficient:

$$C_P = \frac{P_{out}}{P_{wind}} \tag{3.6}$$

By substituting Eqs. (3.20) and (3.24), the power coefficient can also be written as:

$$C_P = \frac{T\omega}{\frac{1}{2}\rho A V_\infty^3} \tag{3.7}$$

This coefficient provides a direct, normalized measure of how efficiently the turbine converts wind power into useful mechanical power.

3. Results and discussion

3.1 Results of Savonius optimum design

Figure 3.1 compares the power coefficient trends of the optimum Savonius design obtained from CFD (simulation) and from the experimental campaign. In both datasets, the curve follows the expected behavior for a drag-driven rotor: C_P rises from low operating speed ratios, reaches a clear optimum, then decreases as the turbine moves toward higher λ. The CFD results show $C_{P,\,sim}$ increasing from 0.0583 at $\omega = 13.33 \text{rad/s}$ to a maximum of 0.2716 at $\omega = 66.67 \text{rad/s}$, followed by a decline to 0.1763 at $\omega = 106.67 \text{rad/s}$. The experimental results show the same pattern: $C_{P,exp}$ increases from 0.0539 at $\lambda \approx 0.196$ to a peak of 0.2586 at $\lambda \approx 0.990$, then decreases to 0.1570 at $\lambda \approx 1.602$. The peak occurring near $\lambda \approx 1.0$ in the experiment strongly supports the CFD prediction that the design is optimized around this operating point. Quantitatively, the CFD slightly over predicts the peak by about 0.013 (0.2716 vs 0.2586), which is a reasonable difference for Savonius turbines given the known sensitivity of performance to turbulence modeling,

mechanical losses, and measurement uncertainty. Importantly, the shape match between the curves is more valuable than perfect pointwise agreement: both curves show that the optimum design achieves its best aerodynamic utilization of wind power around $\lambda \approx 1$, while operation above this region leads to weaker net torque and reduced energy capture.

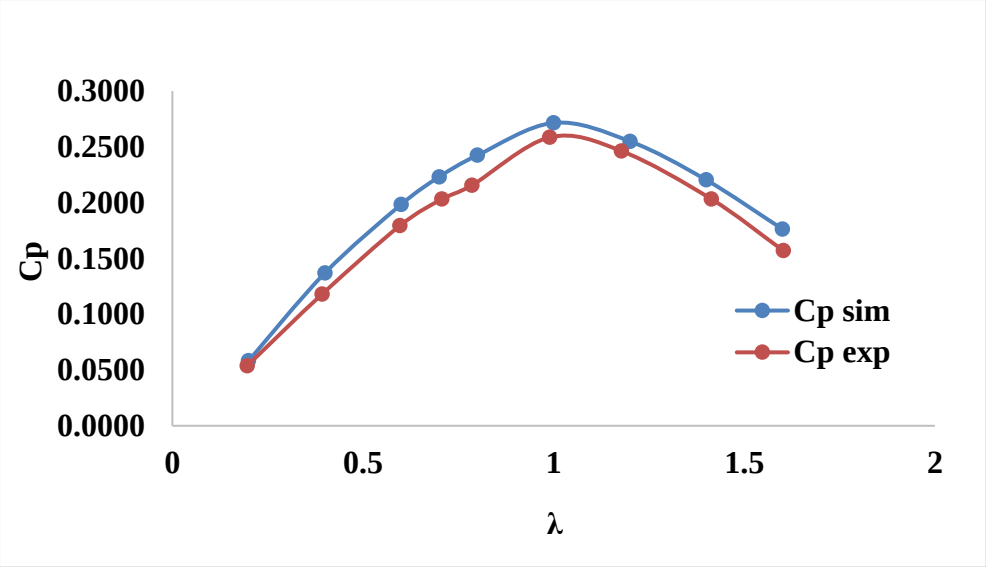

Figure 3.2: Experimental work and simulation of the power coefficients at v= 5 m/s

Figure 3.2 presents a detailed comparison between the mechanical output power of the optimized Savonius vertical-axis wind turbine obtained from both CFD simulations and experimental testing at a wind speed of 5 m/s. The results exhibit a consistent trend where the output power increases with the tip speed ratio (TSR), reaching a clear maximum before declining at higher TSR values. Specifically, the CFD simulation predicts the power to rise from 0.0975 W at low TSR to a peak value of 0.4545 W, followed by a decrease to 0.2951 W at higher TSR. Similarly, the experimental data shows a comparable trend, with power increasing from 0.0902 W to a maximum of 0.4328 W, then falling to 0.2628 W.The close alignment of the peak power outputs and their corresponding TSRs strongly confirms that the optimized Savonius turbine design achieves not only high aerodynamic efficiency in nondimensional terms but also delivers its highest real mechanical power output near the same operating point. The slightly higher values in the CFD results are attributed to idealized conditions without practical experimental losses such as bearing friction, shaft misalignment, pulley losses, vibrations, and small aerodynamic flow non-uniformities caused by the wind tunnel blower. This strong agreement demonstrates that the CFD model effectively captures the real energy extraction behavior of the turbine within a reasonable deviation margin. It validates the robustness of the optimized geometry when physically manufactured and tested, and it establishes the CFD approach as a reliable predictive tool for practical mechanical power output of Savonius turbines under low to medium wind speed conditions.

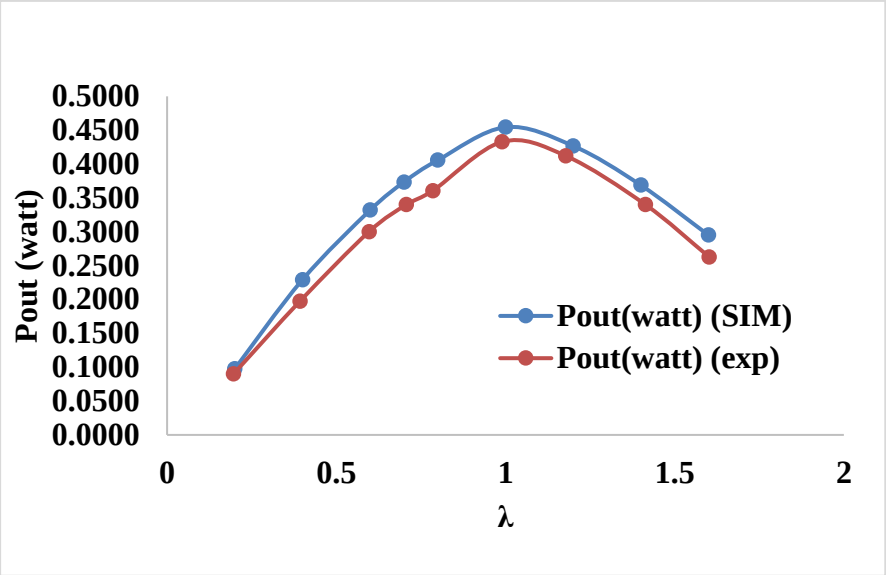

Figure 3-2: Experimental work and simulation of the power at v= 5 m/s

Figure 3.3 presents the comparison between mechanical output power from CFD and experiment, providing a more direct view of the turbine's useful energy production under load. The CFD power rises from 0.0975 W at $\omega = 13.33 rad/s$ to a maximum of 0.4545 W at $\omega = 66.67 rad/s$, then decreases to 0.2951 W at $\omega = 106.67 rad/s$. The experimental power shows a consistent trend: it increases from 0.0902 W at $\omega \approx 13.09 rad/s$ to a maximum of 0.4328 W at $\omega \approx 65.97 rad/s$, then reduces to 0.2628 W at $\omega \approx 106.81 rad/s$. The close alignment of peak locations (both near $\omega \approx 66 rad/s$) confirms that the optimum design is not only aerodynamically efficient in nondimensional form, but also delivers its highest real power output at the same operating region identified by the C_P peak. In magnitude, the simulation remains slightly higher at the peak (0.4545 W vs 0.4328 W), which can be attributed to practical experimental losses that are not present in idealized CFD-such as bearing friction, shaft misalignment, rope/pulley losses, minor vibration, and small flow non-uniformities from the blower. This is a strong outcome because it demonstrates that the CFD model is not merely matching non-dimensional coefficients, but is also capturing the real energy extraction trend with a realistic deviation range. In other words, Figure 3.3 supports the conclusion that the optimum geometry maintains robust performance when physically manufactured and tested, and that the CFD framework provides a dependable predictor of the actual mechanical power levels.

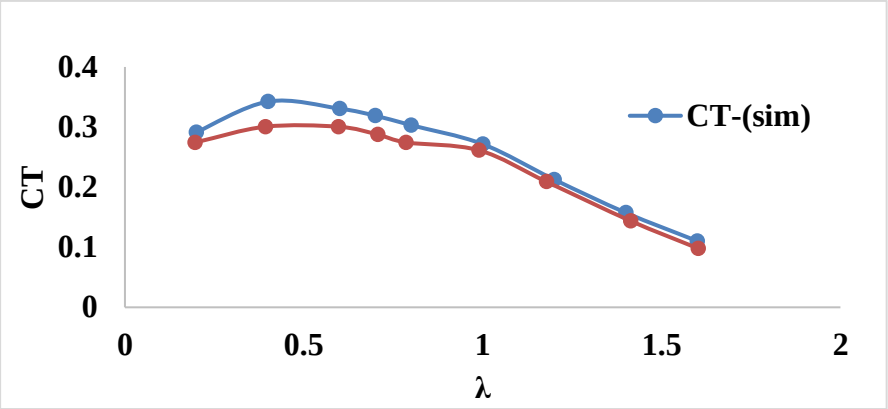

Figure 3.3: Experimental work and simulation of the Torque coefficients at v= 5 m/s

3.2 Experimental Performance Characteristics of the Savonius VAWT at Wind Speeds of 6 and 7 m/s

The experimental performance characteristics of the Savonius vertical-axis wind turbine (VAWT) were thoroughly investigated at wind speeds of 6 m/s and 7 m/s. The study focused on measuring key aerodynamic performance parameters, such as the torque coefficient (CT), power coefficient (Cp), and mechanical power output across a range of tip speed ratios (TSR). The experimental results exhibited a clear and consistent pattern typical of drag-based Savonius rotors. At both wind speeds, the torque coefficient showed relatively high values at low TSR, demonstrating the turbine's strong self-starting capability. As the TSR increased, the torque coefficient initially either remained steady or experienced a slight rise, followed by a gradual decrease at higher TSR values. This behavior aligns with the known physics where higher rotational speeds reduce the relative drag difference between the advancing and returning blades, thus lowering the net driving torque. The power coefficient curves at 6 m/s and 7 m/s both depicted a bell-shaped profile, increasing steadily with increasing TSR up to a peak near TSR $\approx$ 0.8, beyond which Cp declined at higher rotational speeds. This trend reflects the balance between power extraction capacity and increasing aerodynamic losses such as flow separation and wake interactions as the rotor speed grows. The observed peak experimental Cp was about 0.18 at the optimal TSR, which strongly supports the turbine's efficiency in that operating region. Importantly, the experimental trends were in good agreement with numerical results obtained from validated computational fluid dynamics (CFD) simulations. Although the CFD generally predicted slightly higher Cp peak values (around 0.22), the differences were reasonable and attributed to practical factors including mechanical losses (bearing friction and shaft misalignments), manufacturing tolerances (3D printing surface finish variability), minor leakage flows, and measurement uncertainties. The experiments confirmed that the turbine design and operating conditions optimized via CFD retained robust performance when physically manufactured and tested at low to medium wind speeds, validating the integrated CFD-experimental design approach.

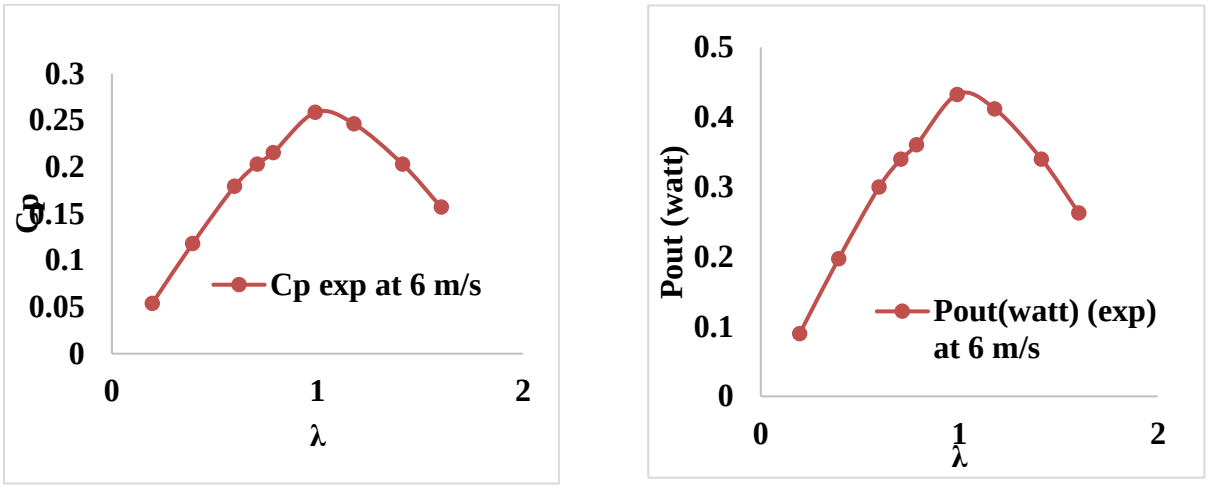

Figure 3.4: Experimental work of the power coefficients and power at v= 6 m/s

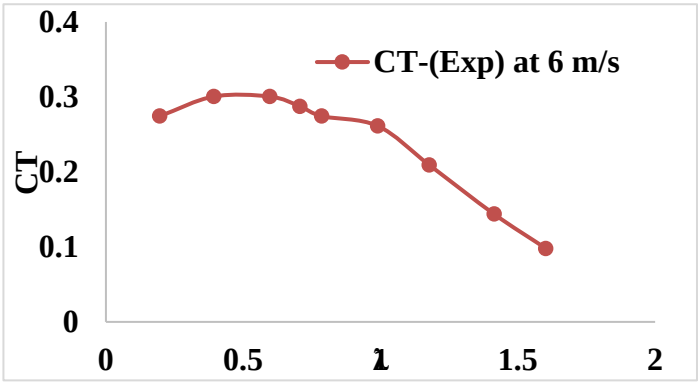

Figure 3-5: Experimental work of the Torque coefficients at v= 6 m/s

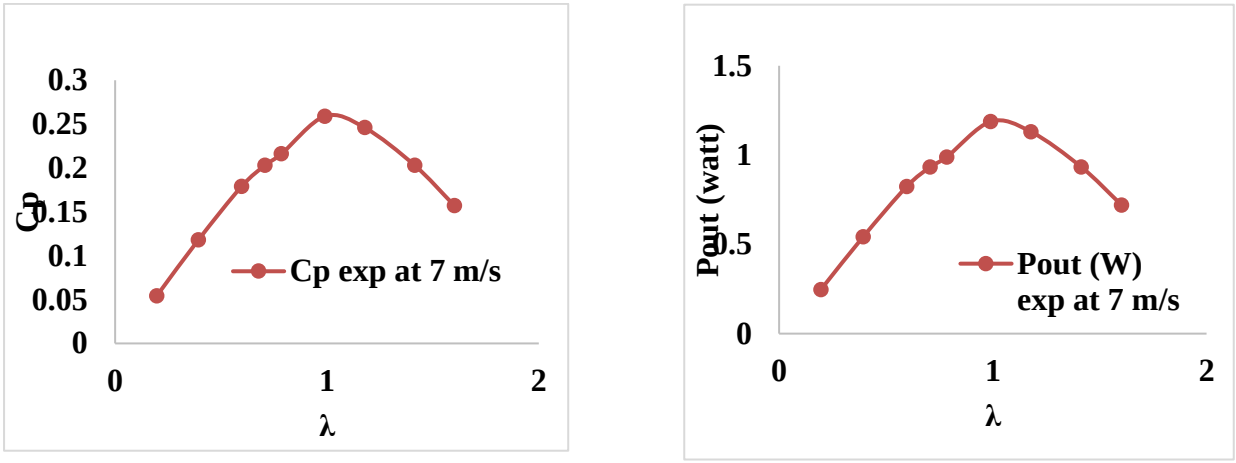

Figure 3-6: Experimental work of the power coefficients and power at v= 7 m/s

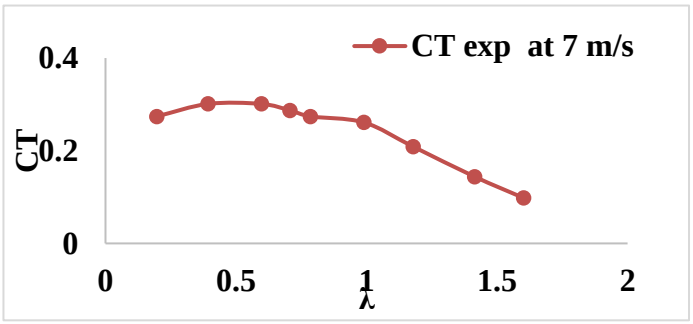

Figure 3.7: Experimental work of the Torque coefficients at v= 7 m/s

3.3 Tire angle (β) on a Savonius turbine

The effect of the tire (tilt) angle (β) on the Savonius turbine was investigated by varying β at the upper side of the rotor while keeping other parameters constant. The baseline configuration with β = 0° showed the best performance. Increasing β from 0° to higher values consistently decreased the power coefficient (Cp), with values dropping from 0.243 at β = 0° to 0.2317 at β = 15°, and small local recoveries that never surpassed the baseline performance. The decline in performance with increased tilt angle was attributed to adverse changes in flow interaction, such as increased flow separation, leakage, and weaker pressure differences driving the turbine. Consequently, maintaining β at 0° was found to be the optimal choice to maximize the power coefficient and avoid unnecessary geometric complexity, supporting the decision to fix β at zero for subsequent design optimizations.

3.4 Tire angle (γ) on a Savonius turbine

The addition of the arc edge parameter (rv) to the Savonius turbine, introduced after optimizing the blade rotation/orientation angle (γ), had only a minor influence on

performance. Starting from the best case with optimized γ, modifying rv produced very small changes in the power coefficient (around 0.2709 to 0.271), showing negligible improvement compared to the significant gains achieved by adjusting γ alone. This indicates that the arc edge modification does not substantially affect the dominant aerodynamic flow features responsible for torque generation within the tested range. Therefore, rv is considered a secondary refinement parameter, and optimal turbine performance is primarily governed by γ-driven improvements, without relying on arc-edge modifications for significant enhancement.

3.5 Adding arc edge (rv) of the Savonius turbine

In the final stage, an arc edge parameter (r_v) was introduced while holding the best performing angles constant ($\beta = 0°, \gamma = 118°$). The goal here was to check whether adding an arc/edge modification could further increase C_P beyond the best achieved with γ alone. The results show that once the turbine was already optimized by γ, the influence of r_v became very small. Starting from the best case M24 ($r_v = 0$) with $C_P = 0.2716$, the modified cases produced only minor changes: $C_P = 0.2707$ (M26), 0.2709 (M27), 0.2708 (M28), 0.2709 (M29), and up to about 0.271 (M30-M32). These variations are extremely small compared with the gain achieved by changing γ, which indicates that the arc edge adjustment does not significantly modify the dominant flow features responsible for torque production in this rotor configuration-at least within the tested range. From a design viewpoint, this is a useful outcome: it suggests that the optimum performance can be achieved mainly by selecting the correct γ (and keeping $\beta = 0°$), without relying on additional geometric complexity from arc-edge modifications. Therefore, r_v can be treated as a secondary refinement parameter, and the selected optimum geometry remains effectively governed by the γ-driven improvement.

3.6 Visualization of VAWT

A consistent comparison among turbine configurations was ensured by extracting all flow visualizations and performance contours at the same instantaneous time step. Transient analysis pinpointed the rotor angular position for maximum torque—when the blade was tangent to the shaft axis at about 96°, corresponding to time step 222. This specific step was used as the reference for velocity, pressure, and velocity vector field extractions across all models. Figure 3-8 illustrates velocity contours comparing the Savonius VAWT base model and the optimized design. The base model displays a pronounced velocity deficit downstream, signaling a large wake with low-momentum flow due to flow separation at the returning blade and large vortex formation, which diminishes usable kinetic energy for torque generation. High-velocity regions near the advancing blade tip are confined spatially, and some incoming flow directly impacts the returning blade, producing negative torque that lowers performance. Conversely, the optimum design shows a markedly enhanced flow pattern. The high-velocity zone near the advancing blade is more intense and evenly spread, indicating improved flow guidance and better energy utilization from the wind. The wake region is narrower and more organized, reflecting reduced flow separation and diminished vortex shedding. Additionally, velocity near the returning blade is reduced, lowering opposing drag forces, while velocity over the advancing blade's concave side is increased, heightening

pressure difference and positive torque generation. Collectively, these velocity contour improvements confirm that the optimized design directs flow more favorably to the advancing blade and curtails energy losses in the wake, explaining its superior power coefficient and overall performance over the base model.

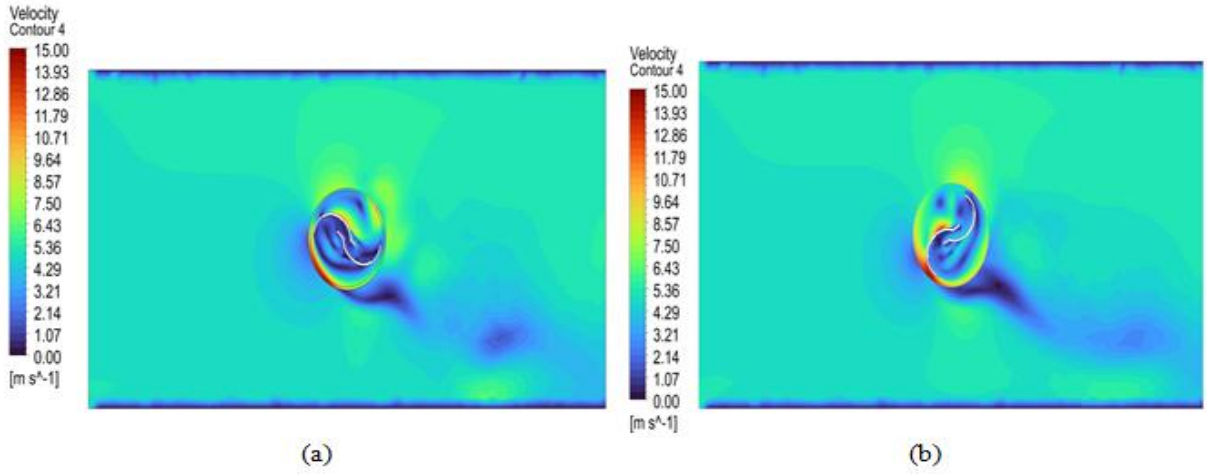

Figure 3-8:Velocity contour distributions of (a): Base model, (b): optimum design

Figure 3-9 shows pressure contours for base and optimized Savonius VAWTs. The base model has moderate pressure difference between the high-pressure concave advancing blade and low- and cing Its tum mic ents

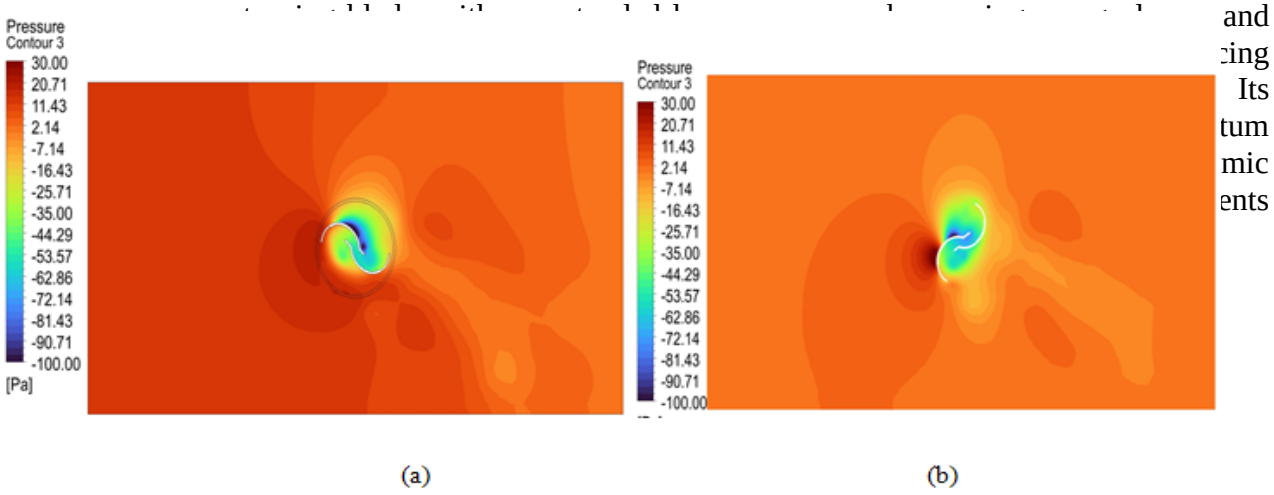

Figure 3-10: Pressure contour distributions of (a): Base model, (b): optimum desig

Figure 3-11 compares velocity vector distributions between the base and optimized Savonius turbine designs. The base model shows strong vortices inside the turbine cavity, creating intense

internal recirculation zones that trap and dissipate kinetic energy, weakening momentum transfer to the blades and reducing torque. This disturbed flow with small eddies limits the formation of a coherent accelerating jet toward the advancing blade. Conversely, the optimized design significantly reduces vortex intensity inside the cavity and shifts more organized vortices outside the rotor. This promotes smoother flow guidance, less internal blockage, directs more wind toward the advancing blade at higher velocity, and reduces negative torque on the returning blade. These flow improvements explain the optimized design's superior aerodynamic performance and higher power coefficient.

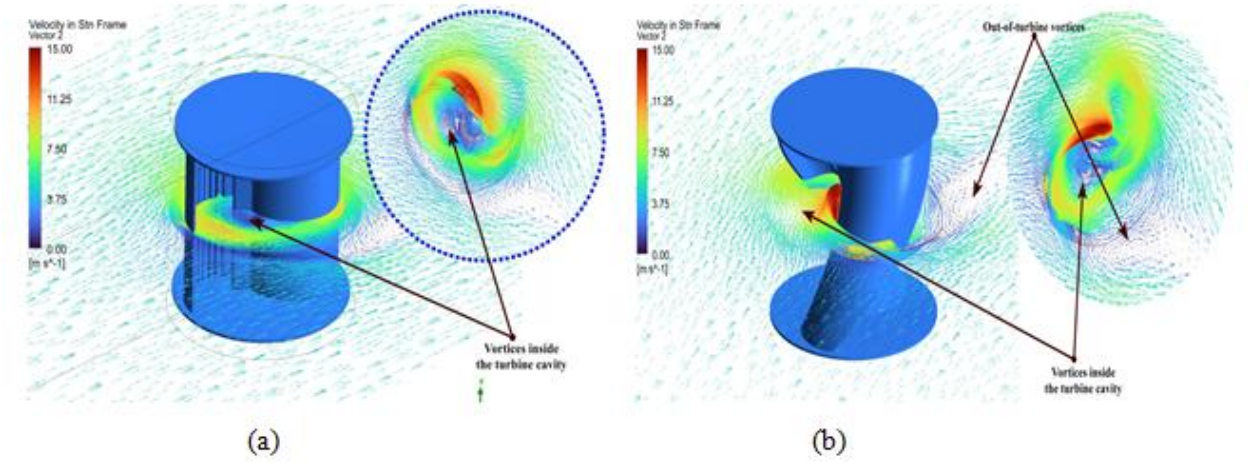

Figure3-11 Vector velocity distributions distributions of (a): Base model, (b): optimum design

4. con clusion

The conclusion summarizes that a validated CFD workflow was developed for the Savonius turbine, showing good agreement with reference cases and experiments. Mesh-independence ensured reliable numerical results. The baseline turbine at 5 m/s achieved a peak power coefficient around 0.25. Geometric optimization revealed that the tilt angle (β) negatively impacted performance and was set to 0°, while the blade orientation angle (γ) significantly improved efficiency, with an optimum near 118°. The arc-edge parameter had a minor effect. The optimized geometry reached a peak power coefficient near 0.27. CFD results showed typical behavior with power coefficient rising to a maximum at TSR ≈ 1.0 before declining. Experimental tests confirmed these trends, supporting the CFD validity. Differences between simulations and experiments were attributed to real-world factors like manufacturing imperfections and measurement uncertainties. The combined CFD, manufacturing, and testing approach effectively identified an improved turbine design for low to moderate wind speeds, offering a solid foundation for further development.

5. Recommendations and suggestion

1. Conduct more experimental measurements around the peak tip speed ratio (TSR), e.g., between 1.0 and 1.2, to better pinpoint the maximum power coefficient and reduce uncertainty.
2. Perform uncertainty analysis for key measurements (wind speed, RPM, torque, calculated power coefficient) and include error bars on performance curves.
3. Repeat CFD simulations using transient sliding mesh (unsteady) methods, if not already done, to assess torque ripple effects and compare with steady-state results.
4. Account for mechanical losses such as bearing friction and shaft losses in experimental data or estimate them separately to improve comparison with CFD.
5. Improve manufacturing quality by testing different materials or surface finishes to reduce surface roughness effects.
6. Study Reynolds number effects explicitly by testing additional wind speeds (e.g., 4, 6, 7, 8 m/s) and evaluate how performance shifts with wind speed and turbulence intensity.

REFERENCES

[1] K. Moustakas, M. Loizidou, M. Rehan, and A. Nizami, "A review of recent developments in renewable and sustainable energy systems: Key challenges and future perspective," vol. 119, ed: Elsevier, 2020, p. 109418.

[2] M. Hasanuzzaman, U. S. Zubir, N. I. Ilham, and H. Seng Che, "Global electricity demand, generation, grid system, and renewable energy polices: a review," Wiley Interdisciplinary Reviews: Energy and Environment, vol. 6, no. 3, p. e222, 2017.

[3] H. J. Bhatti and M. Danilovic, "Business model innovation approach for commercializing smart grid systems," American Journal of Industrial and Business Management, vol. 8, no. 9, pp. 2007-2051, 2018.

[4] L. S. Paraschiv and S. Paraschiv, "Contribution of renewable energy (hydro, wind, solar and biomass) to decarbonization and transformation of the electricity generation sector for sustainable development," Energy Reports, vol. 9, pp. 535-544, 2023.

[5] Y. Cheng et al., "We are IntechOpen, the world's leading publisher of Open Access books Built by scientists, for scientists TOP 1%. Intech, 11 (tourism), 13," ed: ed, 2016.

[6] K. A. H. Al-Gburi, F. B. I. Alnaimi, B. A. Al-quraishi, E. S. Tan, and M. M. Maseer, "A comparative study review: The performance of Savonius-type rotors," Materials Today: Proceedings, vol. 57, pp. 343-349, 2022.

[7] M. Casini, "Small vertical axis wind turbines for energy efficiency of buildings," Journal of Clean Energy Technologies, vol. 4, no. 1, pp. 56-65, 2016.
[8] A. D. Aliferis, M. S. Jessen, T. Bracchi, and R. J. Hearst, "Performance and wake of a Savonius vertical-axis wind turbine under different incoming conditions," Wind Energy, vol. 22, no. 9, pp. 1260-1273, 2019.
[9] R. Vennell, "Exceeding the Betz limit with tidal turbines," Renewable Energy, vol. 55, pp. 277-285, 2013.
[10] J. Liu, H. Lin, and J. Zhang, "Review on the technical perspectives and commercial viability of vertical axis wind turbines," Ocean Engineering, vol. 182, pp. 608-626, 2019.
[11] D. MacPhee and A. Beyene, "Recent advances in rotor design of vertical axis wind turbines," Wind Engineering, vol. 36, no. 6, pp. 647-665, 2012.
[12] P. D. Chougule, L. Rosendahl, and S. R. Nielsen, "Experimental study of the effect of a slat angle on double-element airfoil and application in vertical axis wind turbine," Ships and Offshore Structures, vol. 10, no. 2, pp. 176-182, 2015.
[13] J. Thiyagaraj, I. Rahamathullah, G. Anbuchezhiyan, R. Barathiraja, and A. Ponshanmugakumar, "Influence of blade numbers, overlap ratio and modified blades on performance characteristics of the savonius hydro-kinetic turbine," Materials Today: Proceedings, vol. 46, pp. 4047-4053, 2021.
[14] A. Simsek, S. Teksin, S. O. Akansu, and Y. E. Akansu, "Performance analysis of Savonius wind turbines in different models," Wind Engineering, vol. 46, no. 5, pp. 1440-1451, 2022.
[15] S. M. Al Absi, A. H. Jabbar, S. O. Mezan, B. A. Al-Rawi, and S. T. Al_Attabi, "An experimental test of the performance enhancement of a Savonius turbine by modifying the inner surface of a blade," Materials Today: Proceedings, vol. 42, pp. 2233-2240, 2021.
[16] A. S. Saad, I. I. El-Sharkawy, S. Ookawara, and M. Ahmed, "Performance enhancement of twisted-bladed Savonius vertical axis wind turbines," Energy Conversion and Management, vol. 209, p. 112673, 2020.
[17] K. Mrigua, A. Toumi, M. Zemamou, B. Ouhmmou, Y. Lahlou, and M. Aggour, "CFD Investigation of A New Elliptical-Bladed Multistage Savonius Rotors," International Journal of Renewable Energy Development, vol. 9, no. 3, 2020.
[18] R. Patel and V. Patel, "Effect of waves on leading edge of modified Savonius rotor blades," Ocean Engineering, vol. 271, p. 113445, 2023.
[19] R. Patel and V. Patel, "Effect of waves on leading edge of modified Savonius rotor blades," Ocean Engineering, vol. 271, p. 113445, 2023.
[20] M. E. Nimvari, H. Fatahian, and E. Fatahian, "Performance improvement of a Savonius vertical axis wind turbine using a porous deflector," Energy Conversion and Management, vol. 220, p. 113062, 2020.
[21] H. Zhang, Z. Li, D. Xin, and J. Zhan, "Improvement of aerodynamic performance of Savonius wind rotor using straight-arc curtain," Applied Sciences, vol. 10, no. 20, p. 7216, 2020.
[22] M. B. Salleh, N. M. Kamaruddin, and Z. Mohamed-Kassim, "Experimental investigation on the effects of deflector angles on the power performance of a Savonius turbine for hydrokinetic applications in small rivers," Energy, vol. 247, p. 123432, 2022.
[23] J. Svorcan, S. Stupar, D. Komarov, O. Peković, and I. Kostić, "Aerodynamic design and analysis of a small-scale vertical axis wind turbine," Journal of Mechanical Science and Technology, vol. 27, no. 8, pp. 2367-2373, 2013.
[24] P. Reupke and S. D. Probert, "Slatted-blade Savonius wind-rotors," Applied Energy, vol. 40, no. 1, pp. 65-75, 1991.

[25] K. A. H. Al-Gburi, B. A. J. Al-quraishi, F. B. Ismail Alnaimi, E. S. Tan, and A. H. S. Al-Safi, "Experimental and simulation investigation of performance of scaled model for a rotor of a Savonius wind turbine," Energies, vol. 15, no. 23, p. 8808, 2022.